Journal of Neuroinflammation

RESEARCH

Open Access

m6A-methylase METTL3 promotes retinal angiogenesis through modulation of metabolic reprogramming in RPE cells

Qian Zhou[1†], Xianyang Liu[1,4†], Huiping Lu[1†], Na Li[2], Jiayu Meng[3], Jiaxing Huang[1], Zhi Zhang[1], Jiangyi Liu[1], Wei Fan[1], Wanqian Li[1], Xingran Li[1], Xiaoyan Liu[1], Hangjia Zuo[1], Peizeng Yang[1*] and Shengping Hou[1,4*]

Abstract

Retinal neovascularization (RNV) disease is one of the leading causes of blindness, yet the molecular underpinnings of this condition are not well understood. To delve into the critical aspects of cell-mediated angiogenesis, we analyzed our previously published single-cell data. Our analysis revealed that retinal pigment epithelium (RPE) cells serve a crucial promotional function in angiogenesis. RPE cells were regulated by N6-methyladenosine (m6A). Next, we detected several critical m6A methylase in hypoxic ARPE-19 cells and in oxygen-induced retinopathy (OIR) mice, our results revealed a significant decrease in the level of methyltransferase like 3 (METTL3). METTL3 specific inhibitor STM2457 intravitreal injection or METTL3 conditional knockout mice both showed a significantly reduced neovascularization area of retina. Additionally, the angiogenesis-related abilities of human retinal endothelial cells (HRECs) were diminished after co-cultured with ARPE-19 treated with STM2457 or sh-METTL3 in vitro. Furthermore, through the integration of Methylated RNA immunoprecipitation (MeRIP) sequencing and RNA sequencing, we discovered that the metabolic enzyme quinolinate phosphoribosyltransferase (QPRT) was directly modified by METTL3 and recognized by the YTH N6-methyladenosine RNA binding protein C1 (YTHDC1). Moreover, after over-expressing QPRT, the angiogenic abilities of HRECs were improved through the phosphorylated phosphatidylinositol-3-kinase (p-PI3K)/ phosphorylated threonine kinase (p-AKT) pathway. Collectively, our study provided a novel therapeutic target for retinal angiogenesis.

Keywords Retinal neovascularization, Retinal pigment epithelium, Methyltransferase like 3, Quinolinate phosphoribosyltransferase, p-PI3K/p-AKT pathway

†Qian Zhou, Xianyang Liu, and Huiping Lu have contributed equally to this work.

*Correspondence:
Peizeng Yang
peizengycmu@126.com
Shengping Hou
sphou828@163.com
[1] The First Affiliated Hospital of Chongqing Medical University, Chongqing Key Laboratory of Ophthalmology, Chongqing Eye Institute, and Chongqing Branch (Municipality Division) of National Clinical Research Center for Ocular Diseases, Chongqing 400016, China
[2] Beijing Tongren Hospital, Capital Medical University, Beijing 100730, China
[3] Sichuan Provincial Key Laboratory for Human Disease Gene Study, Sichuan Provincial People's Hospital, University of Electronic Science and Technology of China, Chengdu 611731, China
[4] Beijing Ophthalmology & Visual Sciences Key Laboratory, Beijing Institute of Ophthalmology, Beijing Tongren Eye Center, Beijing Tongren Hospital, Capital Medical University, Beijing 100730, China

© The Author(s) 2024. **Open Access** This article is licensed under a Creative Commons Attribution-NonCommercial-NoDerivatives 4.0 International License, which permits any non-commercial use, sharing, distribution and reproduction in any medium or format, as long as you give appropriate credit to the original author(s) and the source, provide a link to the Creative Commons licence, and indicate if you modified the licensed material. You do not have permission under this licence to share adapted material derived from this article or parts of it. The images or other third party material in this article are included in the article's Creative Commons licence, unless indicated otherwise in a credit line to the material. If material is not included in the article's Creative Commons licence and your intended use is not permitted by statutory regulation or exceeds the permitted use, you will need to obtain permission directly from the copyright holder. To view a copy of this licence, visit http://creativecommons.org/licenses/by-nc-nd/4.0/.

Introduction

Retinal neovascularization (RNV) is a severe complication of eye diseases, including retinopathy of prematurity, age-related macular degeneration, and diabetic retinopathy, which cause severe vision loss and irreversible blindness [1, 2]. Currently, therapeutic methods are limited, and the injection of anti-vascular endothelial growth factor (VEGF) drugs has been widely used in clinical treatment; however, they have many side effects, including physiological angiogenesis suppression, adverse neurodevelopmental outcomes, and VEGF resistance [3–6]. Thus, there is an urgent need to improve our understanding of the mechanisms underlying RNV and identify alternative therapeutic strategies.

Oxygen-induced retinopathy (OIR), a common model used to study RNV, is characterized by excessive oxidative stress and retinal angiogenesis [7]. As the retinal pigment epithelium (RPE) is critical for maintaining retinal homeostasis, the changes it undergoes during OIR have profound implications for the pathological angiogenic process [8]. The RPE is a layer of regular polygonal cells located in an oxygen-rich retinal environment that performs various functions, including metabolism, cytokine secretion, and external blood-retinal barrier (BRB) formation [9–12]. RPE cells are activated quickly to clear excessive reactive oxygen species and maintain the stability of the retinal microenvironment when the retina is disturbed by oxidative damage [13–15]. Additionally, RPE cells secrete numerous cytokines, such as transforming growth factor beta (TGF-β), vascular endothelial growth factor A (VEGFA), and fibroblast growth factor 2 (FGF2), which is critical for the formation of retinal vessels [16, 17].

In our prior research, we discovered that RPE cells exhibit a high degree of plasticity, a feature that is subject to modulation by N6-methyladenosine (m6A) modification [18, 19]. m^6A modification is the most common and reversible modification of eukaryotic mRNA and is regulated by three crucial elements, including writers, erasers, and readers [20, 21]. Writers, such as Methyltransferase like 3 (METTL3) and Methyltransferase like 14 (METTL14), promote methylation. Erasers, such as Fat mass and obesity-associated protein (FTO) and Alk B homolog 5 (ALKBH5), are demethylases. RNA demethylases are highly specific for the type of methylation mark and the location within the RNA molecule that they target. These enzymes can modulate the methylation status of RNA molecules by removing methyl groups in response to cellular signals, thereby playing a role in the dynamic regulation of gene expression [18, 19, 22]. Readers, such as YTH N6-methyladenosine RNA binding protein C 1/2/3(YTHDC1/2/3) and YTH N6-methyladenosine RNA binding protein F1/2/3, can specifically recognize m^6A. By interacting with m6A-modified RNA, these reader proteins can influence the fate of RNA molecules and regulate gene expression [23–25]. All of these are involved in a variety of physiological and pathological processes, such as embryonic development, stem cell differentiation, and tumor progression [26–28]. A previous study found that METTL3 was substantially upregulated in human umbilical vein endothelial cells (HUVECs), and inhibition of METTL3 weakened the proliferation and tube formation abilities of HUVECs [29]. However, whether m6A modification is involved in hypoxia-induced RNV remains unclear.

In our investigation, to identify the crucial methylases involved in OIR, we examined several key methylases and observed a decrease in METTL3 expression during OIR. Both in vitro and in vivo inhibition of METTL3 led to a notable reduction in pathological neovascularization. Further exploration of the mechanisms revealed that METTL3-methylated quinolinate phosphoribosyltransferase (QPRT) was recognized by YTHDC1, and involved in angiogenesis through the phosphorylated phosphatidylinositol-3-kinase (p-PI3K)/ phosphorylated threonine kinase (p-AKT) pathway. These findings position METTL3 as a potential therapeutic target for RNV, opening new avenues for the development of targeted treatments for this condition.

Materials and methods

Cell culture

The ARPE-19 cell line, purchased from the American Type Culture Collection (ATCC, USA), and human retinal endothelial cells (HRECs) were obtained from Procell Life Science&Technology Co.,Ltd., they were grown in Dulbecco's modified Eagle medium supplemented with 1% penicillin–streptomycin solution (Gibco, USA) and 10% fetal bovine serum (Gibco, USA). Passage 2–6, endothelial cells were used. Every cell was cultivated in a humidified, 37 °C, 5% CO_2 environment.

OIR mouse model and primary RPE studies

Adult wild-type C57BL/6 J mice were bought from the Experimental Animal Center of Chongqing Medical University (Chongqing, China). The Ethics Committee of the First Affiliated Hospital of Chongqing Medical University (2019-101) approved the study involving the use of animals. Best1-Cre transgenic mice (created by Beijing View Solid Biotechnology, China) were crossed with floxed Mettl3 mice provided by Professor Xianjun Zhu (Sichuan Provincial People's Hospital) to create Mettl3-conditional knockout (cKO) mice. From postnatal day (P) 7 to P12, C57BL/6 J pups or cKO pups were subjected to a hyperoxia environment (75% oxygen content), and then were brought back to a normoxic environment. On P17, the

mice were euthanized, and the tissues were collected for additional studies.

After being thoroughly cleaned with sterile phosphate buffer saline (PBS) (BL302A, Biosharp) three times, the posterior ocular tissues of mice were digested at 37 °C for 30–35 min with 0.25% trypsin containing EDTA and Phenol red (meilunbio, China). The primary RPE cells of mouse were collected after centrifugation.

Hematoxylin and eosin (H&E) staining

After sacrifice, the eyeballs were harvested immediately from mice, fixed with formalin and embedded in paraffin. The tissues were initially dehydrated using a series of graded alcohols (70–100%), followed by clarification in xylene, and subsequently embedded in paraffin. The retina was sectioned and the slices were mounted onto slides.

The tissue sections underwent standard H&E staining. Hematoxylin is alkaline and stains the basophilic structure of tissues (such as ribosome, nucleus, and RNA in the cytoplasm) into blue purple. Eosin is acidic and stains the eosinophilic structure of tissues (such as intracellular and intercellular proteins) pink, such that the shape of the entire cell tissue is clearly visible. Following the staining process, the sections were sequentially dehydrated with graded alcohols (70–100%) and cleared in xylene before being examined under a Leica microscope (Germany). On the scale of 100 μm, the cells that penetrated the inner member were counted.

Cell stimulation and lentivirus infection

ARPE-19 cells were cultured in a hypoxia incubator with an oxygen concentration of 1–2% for 24 h to induce hypoxia. Briefly, 2×10^5 ARPE-19 cells were seeded and cultivated in a 6-well plate, and then exposed to sh-NC or sh-METTL3 lentivirus (MOI:30, Shanghai Genechem Co., Ltd.) for 6 h or overnight, depending on the manufacturer's instructions. Images of the cells were taken on day 3 following transfection using a fluorescent microscope (DMIL4000, Leica, Germany). Stably transformed cells were selected by puromycin or neomycin for investigation.

Real-time quantitative polymerase chain reaction (RT-qPCR) and Agarose gel electrophoresis

Total RNA was extracted from RPE cells using Steady-Pure Mag Tissue & Cells RNA Extraction Kit (Accurate Biotechnology (Hunan) Co., Ltd., China) according to the manufacturer's instructions. RNA concentration was measured using a spectrophotometer (Thermo Fisher Scientific. Inc., MA, USA), and cDNA was synthesized using Evo M-MLV Mix Kit with gDNA Clean for qPCR (Accurate Biotechnology (Hunan) Co., Ltd., China). RT-qPCR was performed on the ABI 7500 Real-time PCR System (Applied Biosystems, CA, USA) with SYBR Green Premix Pro Taq HS qPCR Kit (Rox Plus (Accurate Biotechnology (Hunan) Co., Ltd., China) according to the instructions. Relative expression levels were normalized to β-actin levels and determined using the $2^{-\Delta\Delta CT}$ method. Rapid Taq DNA Master Mix (P222, Vazyme, China) was used to amplify target METTL3$^{fl/fl}$ DNA in agarose gel electrophoresis, and Hot Start DNA Polymerase (EP1702, BBI, Canada) was used to amplify target BEST1-CRE DNA. All the primers sequence can be viewed in Supplementary Table 1.

Western blotting

The cells were subjected to lysis using radio immunoprecipitation assay lysis buffer (RIPA, Beyotime, China) containing 1% phenylmethanesulfonyl fluoride (PMSF, Beyotime, China) while being kept on ice. The concentration of proteins was determined using the bicinchoninic acid assay quantification kit (BCA, Beyotime, China) following the provided instructions. Protein samples were separated by sodium dodecyl sulfate polyacrylamide gel electrophoresis and subsequently transferred onto polyvinylidene difluoride membranes (USA). Following a 15-min incubation at room temperature in QuickBlock™ Blocking Buffer (Beyotime, P0235, China), the membranes were subjected to immunoblotting. The immunoblotting process involved incubating the membranes with a primary antibody at 4 °C for 16 h or overnight. Following incubation with secondary antibodies at room temperature for 50 min to 1 h, the blots were developed with an enhanced chemiluminescence kit provided by MCE (USA). Band density was quantified using Image J software and normalized to the expression of β-actin. The primary antibodies utilized in this work have been supplied and are documented in Supplementary Table 2.

m^{6}A RNA quantification assay

m^{6}A quantification was conducted with EpiQuik™ m6A RNA Methylation Quantification Kit (Colorimetric) provided by EpigeenTek (P-9005). This kit contents include wash buffer, binding solution, capture antibody, detection antibody, enhancer solution, developer solution, and stop solution. In short, the positive control sample and negative control sample were used to generate a standard curve according to standard procedures. The RNA samples, including the positive and negative control samples, were applied onto an assay well for analysis subsequent to treatment with the binding solution. After the addition of the detection and capture antibodies, the enhanced solution was added for incubation. Subsequently, the absorbance was determined at 450 nm using the created standard curve.

Cell counting kit-8 (CCK-8) assay

RPE cells were seeded in 96-well plates at a density of 1×10^4 cells per well and incubated overnight and cultured for another 24 h after treatment with different concentrations of STM2457 (T9060, TargetMol, USA). To detect proliferation, the culture medium was substituted with a medium containing CCK-8 reagent (C0005, TargetMol, USA) and incubated for additional 2 h. Absorbance was measured at 450 nm using a microplate reader (Thermo Fisher Scientific. Inc. MA, USA).

5-ethynyl-2´-deoxyuridine (EdU) staining

The proliferation of RPE cells was examined using the BeyoClick™ Edu-555 Cell Proliferation Detection Kit (C0075S, Beyotime, China) in accordance with the guidelines provided by the manufacturer. In brief, following a 24 h co-culture with ARPE-19 cells, HRECs were incubated with a working solution of EdU for 1.5 h. Subsequently, the samples were washed twice with PBS and fixed with a 4% paraformaldehyde solution for 15 min at room temperature. To facilitate permeabilization, a permeabilization buffer (G1204-100 ML, Servicebio, China) was applied for 10 min, followed by three further washes with PBS. The cells were then incubated with Click Additive Solution in the dark for 30 min according to the manufacturer's recommendations. Thereafter, the nucleus was stained for 10 min using 1×Hoechst, and images were captured using a fluorescence microscope (Leica, Germany). During the DNA replication phase, RPE cells exhibit green fluorescence, while their nuclei display blue fluorescence.

Tube-formation assays

Different groups of ARPE-19 cells were counted and evenly seeded in 6-well plates at 5×10^5 cells per well. After 24 h of culture under different stimuli, the supernatant was collected and centrifuged to remove the precipitate and then was used to culture HRECs (5×10^5 cells per well) for 24 h. A growth factor-reduced Matrigel basement membrane matrix (Corning, USA) was carefully thawed on ice and applied to a 96-well plate. Each well received 70 μl of the matrix for polymerization. Briefly, 2×10^4 suspended endothelial cells were put into the Matrigel matrix. Images were captured by a microscope after 6 h of incubation at 37 °C and then examined using ImageJ software.

Transwell assay

The Corning Transwell system with inserts (5 mm pores) was used. HRECs were cultured in a medium supplemented with supernatants obtained from ARPE-19 cells that had been subjected to normoxic, hypoxic sh-NC, and hypoxic sh-METTL3 conditions for 24 h. After the culture, 5×10^4 HRECs from each group were collected and transferred to a serum-free medium for further cultivation in the upper compartment of a Transwell chamber. The lower chamber contained a medium supplemented with 10% fetal bovine serum. Following a 24-h incubation, the ARPE-19 cells were washed with PBS and subsequently fixed with a 4% paraformaldehyde solution (BL539A, Biosharp) for 20 min at ambient temperature. Thereafter, the cells were stained with crystal violet (Beyotime, China) for 15 min. Following three washes with PBS, the cells located in the top chamber were removed. The stained cells were captured by a microscope and quantified by ImageJ (USA).

Enzyme-linked immunosorbent assay (ELISA)

The supernatant of ARPE-19 cells was collected after different treatments for 24 h, and the concentration of VEGFA was detected using an ELISA kit (KHG0111, Thermo Fisher Scientific). The absorbance values at 450 nm were determined using a microplate reader (Thermo Fisher Scientific). Each group had at least three repetitions.

mRNA stability assay

After subjection to hypoxia for 24 h, 5 mg/ml actinomycin D (A1410, Sigma Aldrich, USA) was applied to the ARPE-19 cells for 0, 3, and 6 h. Following RNA extraction, RT-qPCR was applied to assess the relative mRNA expression of each target gene.

RNA immunoprecipitation (RIP)

An RIP Kit (BersinBio, Guangzhou, China) was used here. Cells were cultivated and washed twice with PBS, followed by collection of the cell lysates and addition of YTHDC1 antibody (ab259990, Abcam) or IgG (30000-0-AP, Proteintech) for immunoprecipitation for 16 h. After washing and elution, RNA was collected and subjected to RT-qPCR.

Statistical analysis

Two-tailed Student's t-tests and one-way ANOVA were used for parametric tests. Mann–Whitney U-test were used for non-parametric tests. Statistical significance was determined at the p-value threshold of less than 0.05, with SPSS software utilized for the conduct of these analyses. Figures were created using Prism version 8.0 software (GraphPad, San Diego, USA) and each dataset is given as mean ± SD.

Results

Decreased expression of METTL3 in RPE cells under hypoxia

To delve into the critical aspects of cell-mediated angiogenesis, we analyzed the expression patterns of genes associated with angiogenesis across various cell types, building upon our previous data obtained on the course of embryonic ocular development at 9, 10, 11, 14, 15, 18, 20, 23, and 26 weeks (GSE228370). The results showed that RPE cells had a high expression of angiogenesis-related genes, including *VEGFA*, *VEGFB,* and *FGF2* (Fig. 1A). The data indicated that RPE cells promoted angiogenesis, which is consistent with previous studies [30].

Because of their profound importance in several cell biological processes, such as cell differentiation, fetal development, and angiogenesis, the role of RNA methylation modifications in regulating gene expression and cellular fate is increasingly being acknowledged [31, 32]. Notably, angiogenesis is the key pathological phenotype of RNV. We therefore examined the expression of several critical m^6A-modified enzymes in ARPE-19 cells under normoxia and hypoxia. The mRNA levels of METTL3, FTO, and ALKBH5 were significantly decreased after hypoxia treatment, especially those of METTL3 and FTO (Fig. 1B). Western blotting revealed that METTL3 protein level was significantly decreased (Fig. 1C, D). Additionally, immunofluorescence analysis revealed a decrease in the expression of METTL3 following exposure to hypoxic conditions (Fig. 1E). Next, we established an OIR mouse model and isolated primary RPE cells from the control and OIR mice to verify the expression of METTL3 in vivo. The protein level of METTL3 was also significantly reduced in primary RPE cells isolated from OIR (Fig. 1F, G). Collectively, these results suggested that METTL3 may play a key role in OIR.

Inhibition of METTL3 alleviated neovascularization in OIR

STM2457 is a highly potent and selective first-in-class catalytic inhibitor of METTL3 [33, 34]. To investigate the effect of METTL3 on OIR, P13 OIR mice (mice under relative hypoxia on the first day) were injected with STM2457 at concentrations of 100, 300, 500, 1000, and 2000 μM (Supplementary Fig. 1A). Retinal flat-mount showed that 1000 μM was the optimal concentration. P17 is known as the peak period of angiogenesis; therefore, all mice were sacrificed on P17 [35, 36]. Furthermore, retinal flat-mount showed that the clusters of pathological neovascularization were significantly increased in OIR mice treated with dimethyl sulfoxide (DMSO) compared with those in normal mice (NOR) treated with DMSO. However, after injection of STM2457, the clusters of pathological neovascularization were significantly reduced (Fig. 2A, B). Additionally, H&E staining indicated that the retina thickened, retinal layer was disorganized, the inner border membrane was incomplete, and numerous endothelial cells penetrated the inner border membrane in OIR mice treated with DMSO, whereas the retinal layer was slightly disorganized, the inner border membrane was almost intact, and a few endothelial cells penetrated the inner border membrane in OIR mice treated with STM2457 (Fig. 2C, D).

To further validate the role of METTL3 in OIR, we constructed Mettl3 conditional knockout (Met3 cKO) mice by crossing floxed Mettl3 mice ($Met3^{fl/fl}$) with Best1-Cre transgenic mice (Supplementary Fig. 1B). After inducing OIR in these mice, retinal flat mounts showed that pathological neovascularization was significantly decreased in Met3 cKO mice compared with that of $Met3^{fl/fl}$ mice (Fig. 2E, F). Moreover, H&E staining revealed fewer endothelial cells penetrating the inner border membrane in Met3 cKO mice than in $Met3^{fl/fl}$ mice, and both the inner border membrane and retina layer were more intact than those in $Met3^{fl/fl}$ mice (Fig. 2G, H).

These results suggest that, despite a decrease in METTL3 levels in the OIR model, it still functioned as a pathogenic gene. Inhibition of METTL3 led to a mitigation of neovascularization and an improvement in local ischemic perfusion within the retina.

Inhibition of METTL3 in ARPE-19 cells attenuated angiogenesis

To investigate the effects of METTL3 in vitro, a METTL3 knockdown lentivirus (sh-METTL3) was constructed. Transfection efficiency in ARPE-19 cells was approximately 90%, indicating successful transfection (Fig. 3A). Approximately 70% knockdown efficiency was observed in ARPE-19 cells transfected with sh-METTL3 (Fig. 3B).

(See figure on next page.)

Fig. 1 Expression of METTL3 in RPE cells under hypoxia. **A** Angiogenesis-associated gene expression across distinct cellular clusters as revealed by single-cell RNA sequencing. **B** mRNA expression of METTL3, METTL14, FTO, and ALKBH5 in ARPE-19 cells with or without hypoxia for 24 h using RT-qPCR (n = 3; mean ± SD; ns > 0.05, *p < 0.05, **p < 0.01; unpaired Student's t-test). **C**, **D** Quantitative levels of the proteins METTL3, METTL14, FTO, and ALKBH5 in the two groups mentioned above (n = 3; mean ± SD; ns > 0.05, *p < 0.05, **p < 0.01; unpaired Student's t-test). **E** Fluorescence intensity and subcellular location of METTL3 (bar: 50 μm). **F**, **G** METTL3 protein level of primary RPE cells isolated from NOR and OIR mice (n = 3; mean ± SD; **p < 0.01; unpaired Student's t-test)

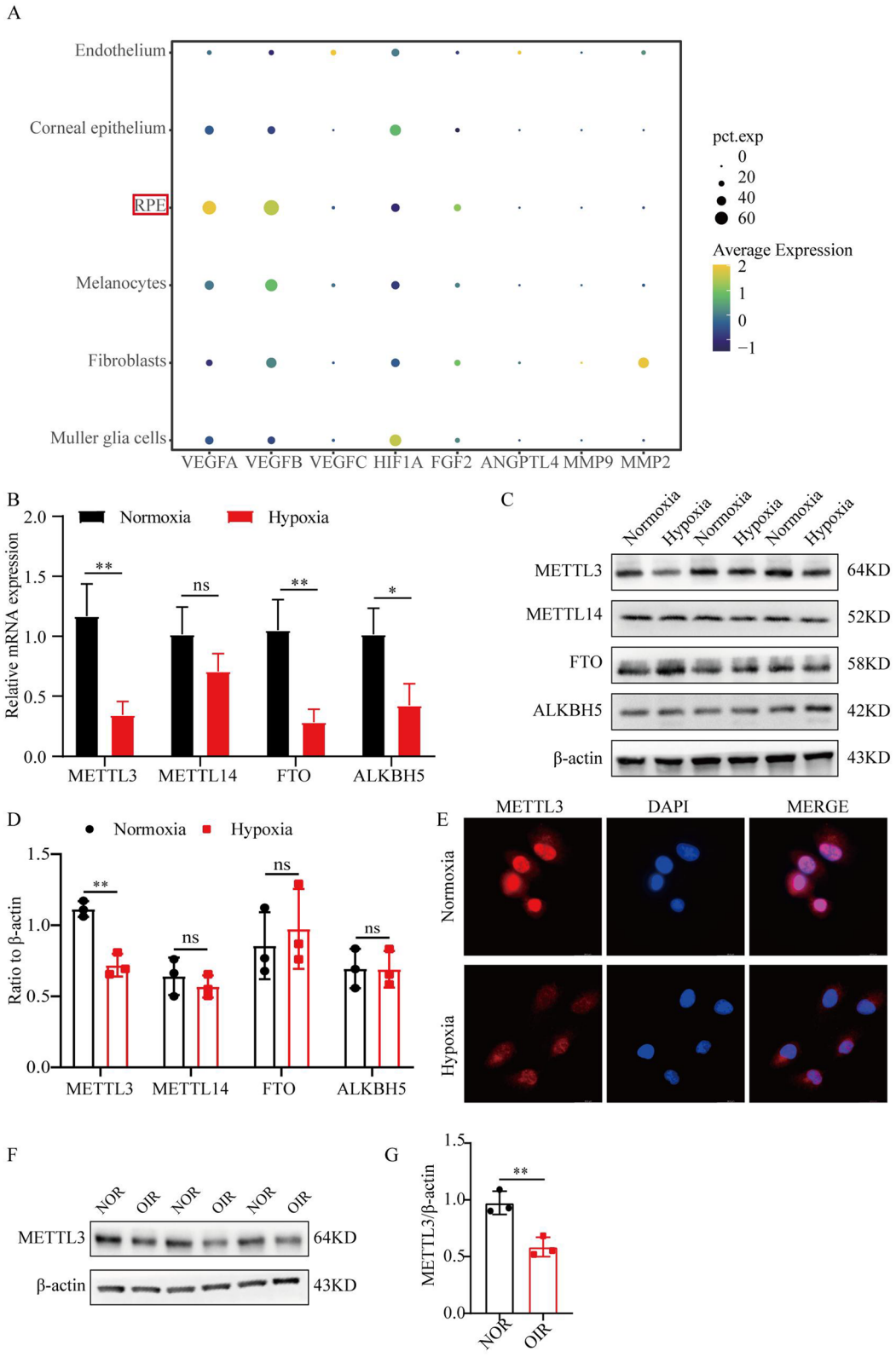

Fig. 1 (See legend on previous page.)

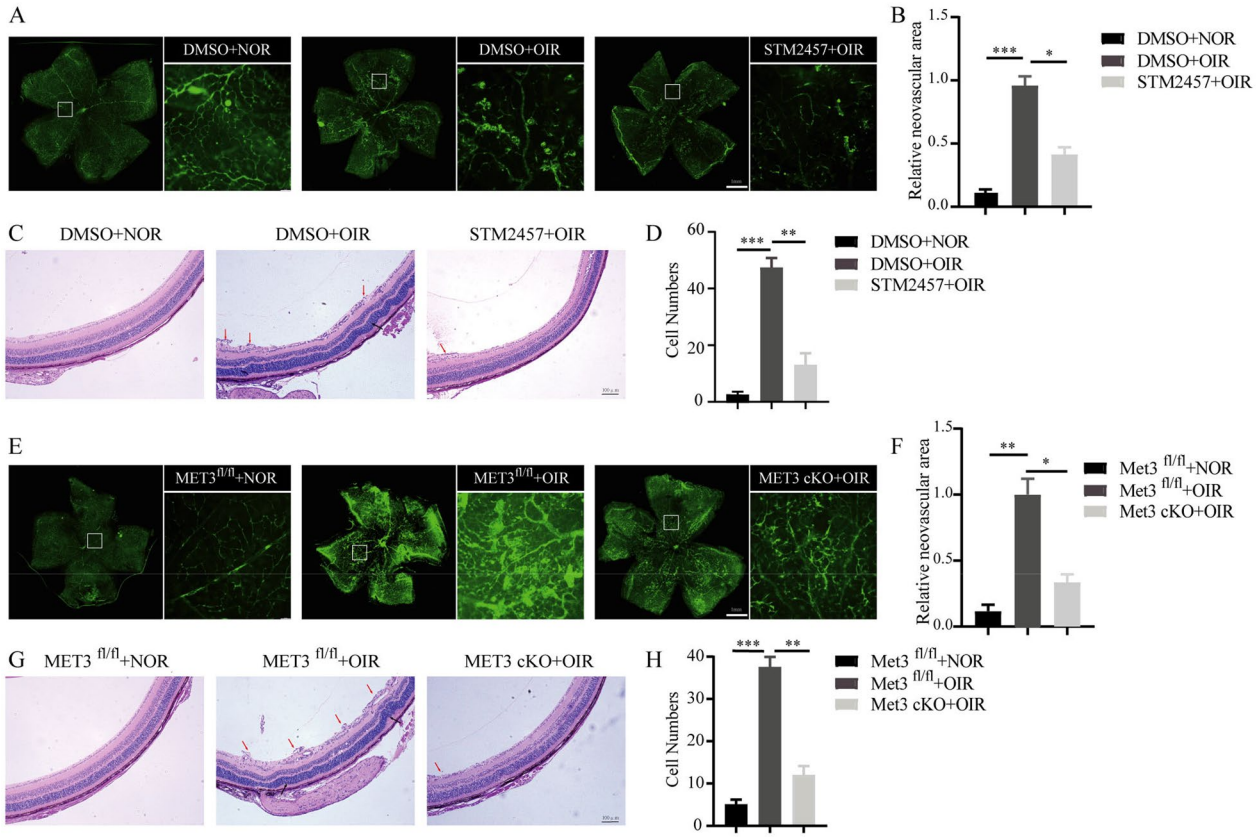

Fig. 2 Attenuated angiogenesis in OIR mice with inhibition or knockout of METTL3. **A**, **B** Representative fluorescein angiography images of retina flat-mounts and percentage of pathological neovascularization area (bar: 1 mm) (n = 3/group; mean ± SD; *p < 0.05, ***p < 0.001; Mann–Whitney U test; the individual experiments were carried out with intervals ranging from 5 days to 2 weeks, each individual experiment was repeated once). **C**, **D** Representative images of histologic sections and corresponding quantifications of cells penetrating the inner limiting membrane. Red arrows, endothelial cells penetrating the inner limiting membrane; Black arrows, disorganized retinal layers (bar: 100 μm) (n = 3/group; mean ± SD; **p < 0.01, ***p < 0.001; Mann–Whitney U test; the individual experiments were executed with intervals varying from 1 week to half a month, each individual experiment was repeated once). **E**, **F** Representative retina flat-mounts and percentage of pathological neovascularization area in NOR METTL3$^{fl/fl}$, OIR/METTL3$^{fl/fl}$, and OIR METTL3 cKO mice (bar: 1 mm) (n = 3/group; mean ± SD; *p < 0.05, **p < 0.01; Mann–Whitney U test; the individual experiments were carried out with intervals ranging from 5 days to 2 weeks, each individual experiment was repeated once). **G**, **H** Representative images of histologic sections and corresponding quantifications of cells penetrating the inner limiting membrane in NOR METTL3$^{fl/fl}$, OIR METTL3.$^{fl/fl}$, and OIR METTL3 cKO mice. Red arrows, endothelial cells penetrating the inner limiting membrane; Black arrows, disorganized retinal layers (bar: 100 μm) (n = 3/group; mean ± SD; **p < 0.01, ***p < 0.001; Mann–Whitney U test; the individual experiments were executed with intervals varying from 1 week to half a month, each individual experiment was repeated once)

(See figure on next page.)

Fig. 3 Reduced angiogenesis-related abilities in METTL3-silenced ARPE-19 cells under hypoxia. **A** Transfection efficiency of the METTL3-silenced lentivirus in ARPE-19 cells (BF, bright field; EGFP, enhanced green fluorescence protein; bar: 200 μm). **B** METTL3 protein level and quantification in control and METTL3-silenced ARPE-19 cells (n = 3; mean ± SD; **p < 0.01; unpaired Student's t-test). **C** m^{6}A % in ARPE-19 cells with control or siMETTL3 (n = 3; mean ± SD; **p < 0.01; unpaired Student's t-test). **D**, **G** Percentage of EdU-positive cells in ARPE-19 cells with control vector under normoxia or hypoxia, and in those with siMETTL3 under hypoxia (bar: 100 μm) (n = 3/group; mean ± SD; *p < 0.05, **p < 0.01; Mann–Whitney U test; the individual experiments were executed with intervals varying from 3 day to 1 week, each individual experiment was repeated once). **E**, **H** Transwell images and quantification of the above three groups (bar: 100 μm) (n = 3/group; mean ± SD; *p < 0.05, ***p < 0.001; Mann–Whitney U test; the individual experiments were executed with intervals varying from 3 day to 1 week, each individual experiment was repeated once). **F**, **I** Representative images and quantitation of HREC tube formation (bar: 100 μm) (n = 3/group; mean ± SD; **p < 0.01, ***p < 0.001; Mann–Whitney U test; the individual experiments were executed with intervals varying from 3 day to 1 week, each individual experiment was repeated once). **J** Protein levels and quantitative chart of HIF-1α, FGF2, ANGPTL4, MMP2, and MMP9 in ARPE-19 cells with or without siMETTL3 under hypoxia (n = 3; mean ± SD; *p < 0.05, **p < 0.01, ***p < 0.001; unpaired Student's t-test;). **K** Cell viability of ARPE-19 cells after STM2457 treatment for 24 h at a series of concentrations by CCK-8 assay (n = 5; mean ± SD; *p < 0.05; one-way ANOVA). **L** The overall m^{6}A% in ARPE-19 cells treated with DMSO or STM2457 (n = 3; mean ± SD; *p < 0.05; unpaired Student's t-test). **M** Western blotting for detecting the relative expression of HIF-1α, FGF2, ANGPTL4, MMP2, and MMP9 (n = 3; mean ± SD; *p < 0.05, **p < 0.01; unpaired Student's t-test;)

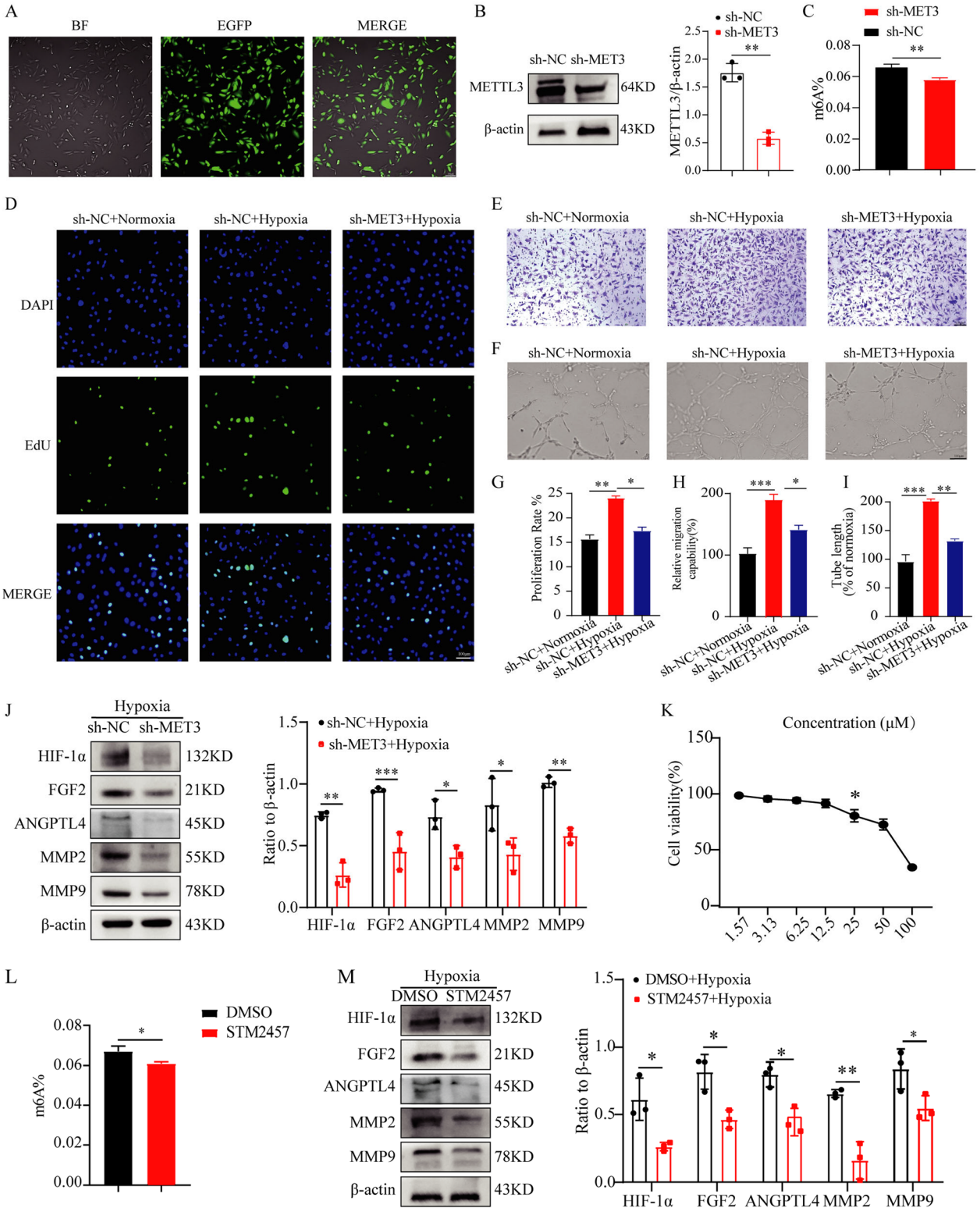

Fig. 3 (See legend on previous page.)

The overall m^6A modification rate was significantly decreased after METTL3 silencing (Fig. 3C). To investigate the effect of RPE cells on endothelial cells, the supernatant of ARPE-19 cells subjected to normoxia or hypoxia was collected and used to culture HREC cells for 24 h. The results showed that tube formation, migration, and proliferation were significantly increased in the hypoxia-treated ARPE-19 group compared with those in the normoxia-treated ARPE-19 group; after the knockdown of METTL3, these processes were significantly decreased (Fig. 3D–I). Subsequently, we detected molecular-level changes in ARPE-19 cells. After hypoxia treatment, the levels of vascular-related proteins, including hypoxia inducible factor 1 subunit alpha (HIF-1α), FGF2, angiopoietin like 4 (ANGPTL4), matrix metallopeptidase 2 (MMP2), and matrix metallopeptidase 9 (MMP9), were significantly decreased in METTL3 knockdown ARPE-19 cells (Fig. 3J). ELISA showed decreased secretion of VEGFA in sh-METTL3-treated ARPE-19 cells under hypoxic conditions (Supplementary Fig. 2). Taken together, these results revealed that the inhibition of METTL3 in ARPE-19 cells obviously decreased angiogenic activity.

Furthermore, ARPE-19 cells were treated with STM2457 for 24 h. Cell viability assay showed that 12.5 μM was the optimal concentration (Fig. 3K). Moreover, the overall m6A modification rate was significantly decreased after treatment with STM2457 (Fig. 3L). Subsequently, the levels of vascular-related proteins were examined. The results showed that the protein levels of HIF-1α, FGF2, MMP2, and MMP9 were significantly decreased in STM2457-treated ARPE-19 cells with hypoxia (Fig. 3M). In conclusion, our findings show that the suppression of METTL3, through inhibition of its expression or activity in ARPE-19 cells, results in a significant downregulation of proteins critical to vascular function. This observation suggests that the suppression of METTL3 in these cells effectively mitigates disruptions in angiogenic processes.

QPRT was directly modified by METTL3

To investigate the downstream targets modified by METTL3 in RPE cells, we performed m^6A methylation-sensitive RNA immunoprecipitation sequencing (MeRIP-seq) and RNA sequencing (RNA-seq) on siMETTL3-treated ARPE-19 cells [19]. Gene Ontology analysis revealed that the differentially expressed genes were mostly enriched in metabolism-related pathways (Fig. 4A). Particularly, we found that QPRT m^6A modification decreased most significantly compared to that of other genes and was implicated in metabolic processes. Therefore, we focused on QPRT for further study.

QPRT, a key enzyme involved in the de novo synthesis of NAD (+), mediates a critical process in tryptophan metabolism [37]. It is also an independent predictor of breast cancer prognosis and promotes tumor neovascularization [38, 39]. We verified whether QPRT played a role in RPE cells after METTL3 inhibition under hypoxic conditions. We found that QPRT expression was significantly reduced in STM2457-treated and METTL3-silenced ARPE-19 cells under hypoxic conditions (Fig. 4B; Supplementary Fig. 3A). Additionally, the m^6A modification of QPRT mRNA was significantly downregulated in METTL3-silenced ARPE-19 cells (Fig. 4C). To validate this result, we performed a MeRIP-qPCR assay and found that m^6A modification of QPRT mRNA was significantly decreased in METTL3-silenced ARPE-19 cells following hypoxic stimulation (Fig. 4D). Furthermore, we performed mRNA stability assays and found that the half-life of QPRT mRNA was shorter in METTL3-silenced ARPE-19 cells than in the control group under hypoxia, suggesting that METTL3 influenced QPRT expression through regulation of mRNA stability under hypoxia (Fig. 4E).

The YTH family is a crucial family of m^6A readers that can target thousands of mRNAs by recognizing m^6A motifs; therefore, we predicted the binding potential of YTH family members to QPRT mRNA using the POSTAR3 website and identified that the YTHDC1 protein could bind specifically to QPRT mRNA [40, 41]. We transfected YTHDC1 lentiviruses (shYTHDC1-1,2,3) and the corresponding vectors into ARPE-19 cells and selected shYTHDC1-3 cells with the highest knockdown efficiency for further experiments (Supplementary Fig. 3B, C). After silencing YTHDC1, the protein levels of QPRT were significantly reduced under hypoxic conditions (Fig. 4F). We then performed RIP assay, and the results showed significant enrichment between YTHDC1 and QPRT compared to that in the IgG control group, suggesting that QPRT was specifically recognized by and bound to YTHDC1 (Fig. 4G). Collectively, these findings suggested that METTL3 regulated QPRT mRNA expression in a YTHDC1-dependent manner.

Overexpression of QPRT promoted retinal angiogenesis

To further verify the role of METTL3-modified QPRT, we overexpressed QPRT (oe-QPRT) in METTL3-silenced ARPE-19 cells under hypoxic conditions. The transfection efficiency reached > 80%, and the overexpression of QPRT was approximately sixfold compared to that of the vehicle (Fig. 5A, B). Our phenotypic analysis showed a marked enhancement in tube formation, migration, and proliferation abilities in METTL3-silenced ARPE-19 cells overexpressing QPRT (oe-QPRT) under hypoxic conditions (Fig. 5C–H). Subsequent study of the protein levels of key vascularization-related molecules, including

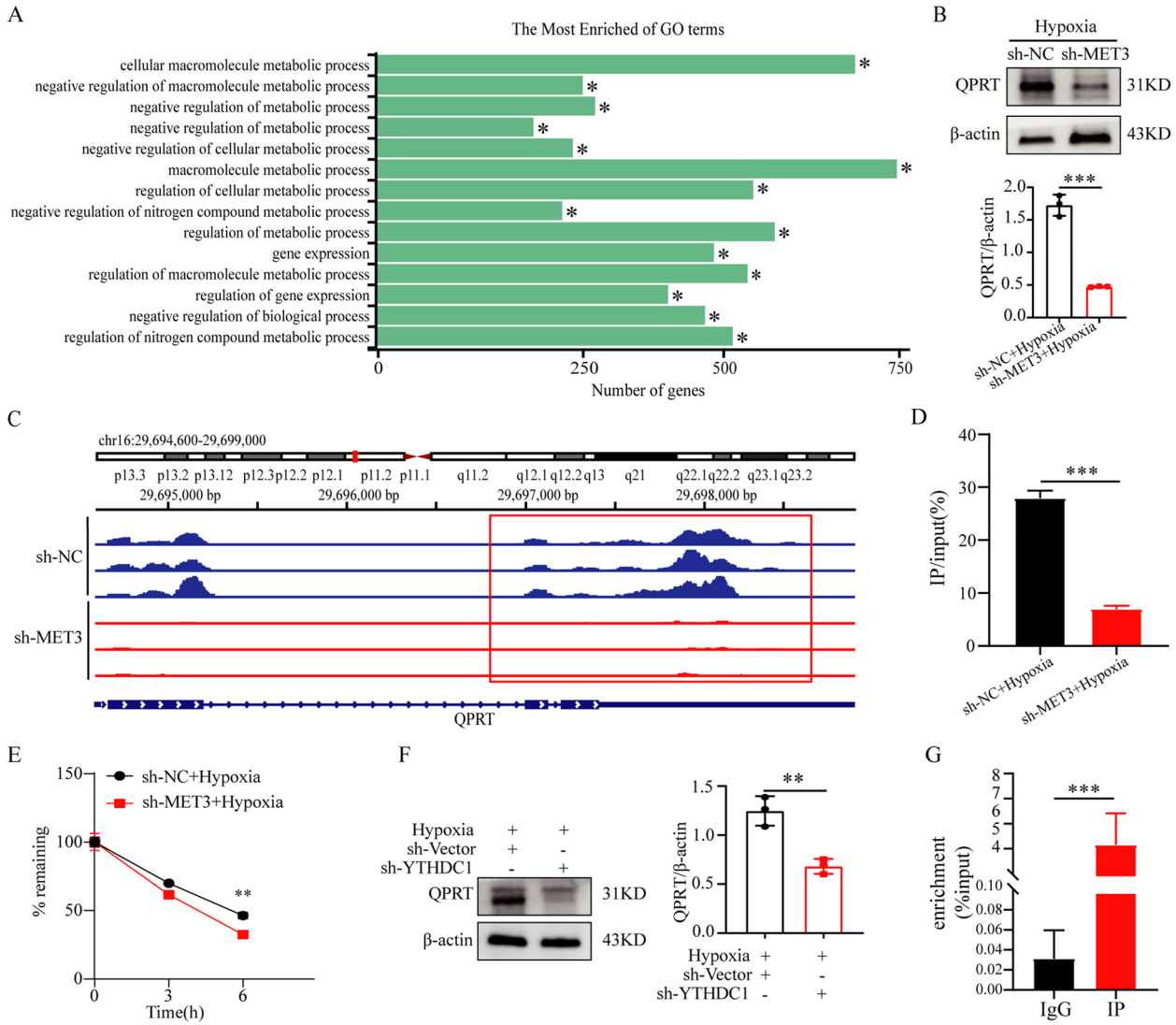

Fig. 4 QPRT is regulated by METTL3 in a YTHDC1-dependent manner. **A** Gene Ontology analysis of differentially expressed genes. **B** QPRT protein expression of control and METTL3-silenced ARPE-19 cells under hypoxia. (n = 3; mean ± SD; ***p < 0.001; unpaired Student's t-test;). **C** IGV map of QPRT by MeRIP-seq. **D** MeRIP-qPCR of QPRT in ARPE-19 cells with control or sh-METTL3 under hypoxia. (n = 3; mean ± SD; ***p < 0.001; unpaired Student's t-test). **E** Detection of half-life of QPRT mRNA in ARPE-19 cells with control or siMETTL3 after hypoxia stimulation (n = 3; mean ± SD; **p < 0.01; unpaired Student's t-test). **F** Representative western blotting images of QPRT in the control and YTHDC1-silenced groups under hypoxia. (n = 3; mean ± SD; **p < 0.01; unpaired Student's t-test). **G** RIP assay of QPRT after IgG and YTHDC1 immunoprecipitation. (n = 3; mean ± SD; ***p < 0.001; unpaired Student's t-test)

HIF-1α, FGF2, ANGPTL4, MMP2, and MMP9, revealed a significant upregulation in METTL3-silenced ARPE-19 cells with oe-QPRT, compared to that in cells treated with the vehicle under hypoxic conditions (Fig. 5I). These findings suggest that QPRT modulates the expression of these proteins associated with angiogenesis. Moreover, ELISA results indicated a substantial increase in VEGFA secretion in METTL3-silenced ARPE-19 cells with oe-QPRT under hypoxic conditions (Supplementary Fig. 4). Collectively, these findings suggest that the QPRT, downstream of METTL3, exacerbates angiogenesis through the induction of these vascular-related proteins within ARPE-19 cells.

METTL3-modified QPRT regulated angiogenesis through the p-PI3K/p-AKT signaling pathway

QPRT participates in cancer development via the PI3K/AKT pathway [42, 43]. KEGG analysis of our MeRIP-seq data also revealed that the PI3K/AKT pathway was significantly enriched in METTL3-silenced ARPE-19 cells

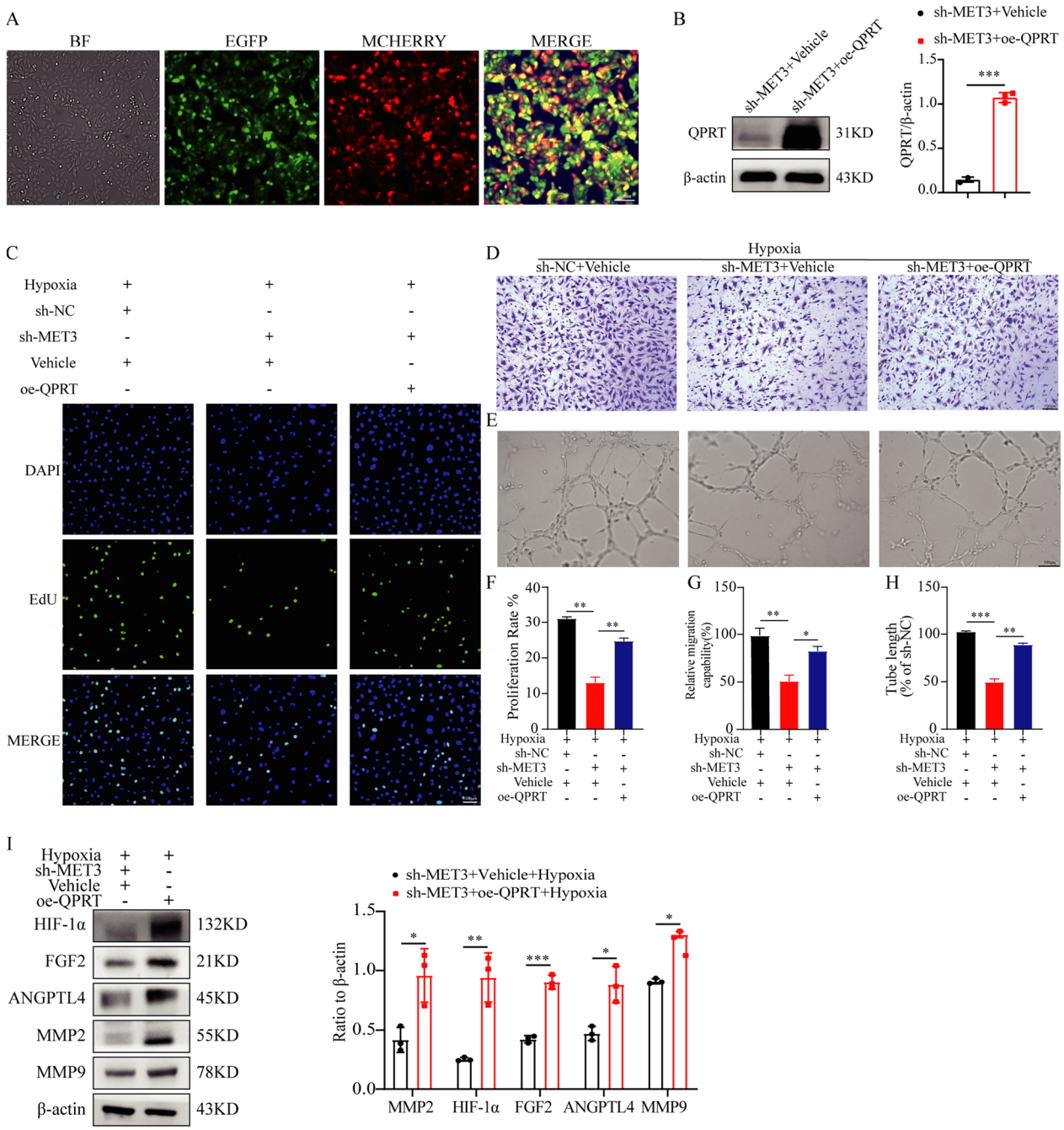

Fig. 5 Enhancement of neovascularization after QPRT overexpression. **A** Co-transfection of METTL3-silenced and QPRT-overexpressed lentivirus (BF, bright field; EGFP, enhanced green fluorescence protein; mCHERRY, red; scale bar: 200 μm). **B** Representative western blotting images and quantification of QPRT in control or oe-QPRT group. (n = 3; mean ± SD; ***p < 0.001; unpaired Student's t-test). **C**, **F** Percentage of EdU-positive cells in vector and METTL3-silenced ARPE-19 cells with or without oe-QPRT under hypoxia. (n = 3/group; mean ± SD; **p < 0.01; Mann–Whitney U test; the individual experiments were executed with intervals varying from 5 days to 2 weeks, each individual experiment was repeated once). **D**, **G** Transwell images and corresponding quantification in the above three groups (scale bar: 100 μm) (n = 3/group; mean ± SD; *p < 0.05, **p < 0.01; Mann–Whitney U test; the individual experiments were executed with intervals varying from 5 days to 2 weeks, each individual experiment was repeated once). **E**, **H** Representative images and quantitation of HREC tube formation in the above three groups (scale bar: 100 μm) (n = 3/group; mean ± SD; **p < 0.01, ***p < 0.001; Mann–Whitney U test; the individual experiments were executed with intervals varying from 5 days to 2 weeks, each individual experiment was repeated once). **I** Western blotting for detecting the relative expression of HIF-1α, FGF2, ANGPTL4, MMP2, and MMP9 in METTL3-silenced ARPE-19 cells with vector or oe-QPRT (n = 3; mean ± SD; *p < 0.05, **p < 0.01, ***p < 0.001; unpaired Student's t-test)

(Fig. 6A). Therefore, we explored whether the effects of QPRT were associated with the PI3K/AKT pathway. Western blotting showed that the protein levels of p-PI3K and p-AKT were significantly elevated in METTL3-silenced cells with oe-QPRT compared to those in the vehicle group under hypoxia, and no significant change was observed in PI3K and AKT, indicating that QPRT regulated phosphorylation of the PI3K/AKT pathway (Fig. 6B).

Collectively, our data suggested that METTL3-methylated QPRT was recognized by YTHDC1, and involved in angiogenesis by regulating vascular-related factors and endothelial cell function under hypoxia, which may be mediated through the p-PI3K/p-AKT pathway (Fig. 6C).

Discussion

OIR, a classical RNV model, has been widely used to investigate the pathogenesis and mechanisms underlying RNV. Numerous cell types, including microglia, Müller, and RPE cells, participate in RNV [44–48]. However, the role of the RPE cells in OIR has rarely been reported. RPE cells, located in the oxygen-rich retinal environment, perform a variety of functions, including metabolism, cytokine secretion, and external BRB formation [9]. In our study, using single-cell data, we found that RPE cells highly expressed vascular-related proteins during eye development.

The m6A RNA methylation, being a highly frequent RNA modification in eukaryotic cells, has garnered considerable interest in research pertaining to angiogenesis-related diseases, including malignant tumors and arthritis [49, 50]. m^6A affects all aspects of mRNA metabolism, including stability, translation, localization, and splicing, and plays a key regulatory role in various processes, such as tumor and stem cell differentiation [51, 52]. It was found that m^6A not only affects the initiation and progression of cancer, but also tumor angiogenesis.

In bladder cancer, the knockout of METTL3 in cancer stem cells prevents angiogenesis [53, 54]. It has also been reported that FTO affects choroidal neovascularization by regulating endothelial cell functions in an m^6A-YTHDF2-dependent manner and that METTL3-mediated m^6A modification regulates pathological angiogenesis in the retina and cornea of mice [55].

In the present study, we observed decreased METTL3 expression in RPE cells isolated from OIR mice and in ARPE-19 cells after hypoxic stimulation. Interestingly, after inhibiting it, pathological neovascular clusters were significantly reduced. We speculated that this may be due to a compensatory mechanism in which the body attempts to mitigate the effects of the lesion by reducing METTL3 expression. However, this compensation may not be sufficient to completely prevent the pathological process, so further artificial inhibition of METTL3 may contribute to more effective disease remission. Further investigation into the underlying mechanisms will be conducted in our future studies.

Through integrated analysis by MeRIP-seq and RNA-seq, we identified QPRT as a potential target gene of METTL3. QPRT, a rate-limiting enzyme involved in NAD + generation in the kynurenine pathway, is an independent predictor of breast cancer prognosis and promotes cancer through the PI3K/AKT signaling pathway [39]. The PI3K/AKT signaling pathway plays a vital role in the regulation of METTL3-mediated m^6A modifications in bone marrow mesenchymal stem cells [56]. Rescue experiments and RIP assay indicated that m^6A methylation of QPRT mRNA in ARPE-19 cells was recognized by the reader YTHDC1 under hypoxia, which regulated angiogenesis via the PI3K/AKT signaling pathway. Contrary to previous studies, our results showed that the QPRT-mediated PI3K/AKT pathway in RPE cells does not affect RPE barrier function, but mainly affects angiogenesis [57], highlighting the adaptable nature of RPE cells in various environmental conditions.

Although our study suggests that METTL3 regulates retinal pathological neovascularization by affecting QPRT and acting in an m^6A-dependent manner on the RPE, we recognize that there are some limitations. Additional OIR models and patients with RNV are required to verify our findings. Additionally, m^6A methylation in the OIR mouse model and patients with RNV need to be confirmed. Moreover, although we confirmed that QPRT was directly modified by METTL3, it remains unclear which QPRT motif is the modified site. We detected METTL3 down-regulation in the OIR model; however, how METTL3 expression changes in other RNV models remains unclear. We speculated that METTL3 played a pathogenic role, but there may be a self-regulatory mechanism that downregulates METTL3 to reduce its pathogenic effect; however, its regulatory mechanism remains to be explored. Hypoxia stimulation is one of the pathogenic factors of RNV; thus, other factors, including hyperglycemia, high intraocular pressure, and oxidative stress, may also play key roles in RNV by affecting m^6A methylation [7, 58, 59].

Collectively, our results suggested that METTL3 promoted pathological retinal neovascularization through QPRT in a YTHDC1-dependent manner in RPE cells. This indicates METTL3 as a potential therapeutic target for RNV.

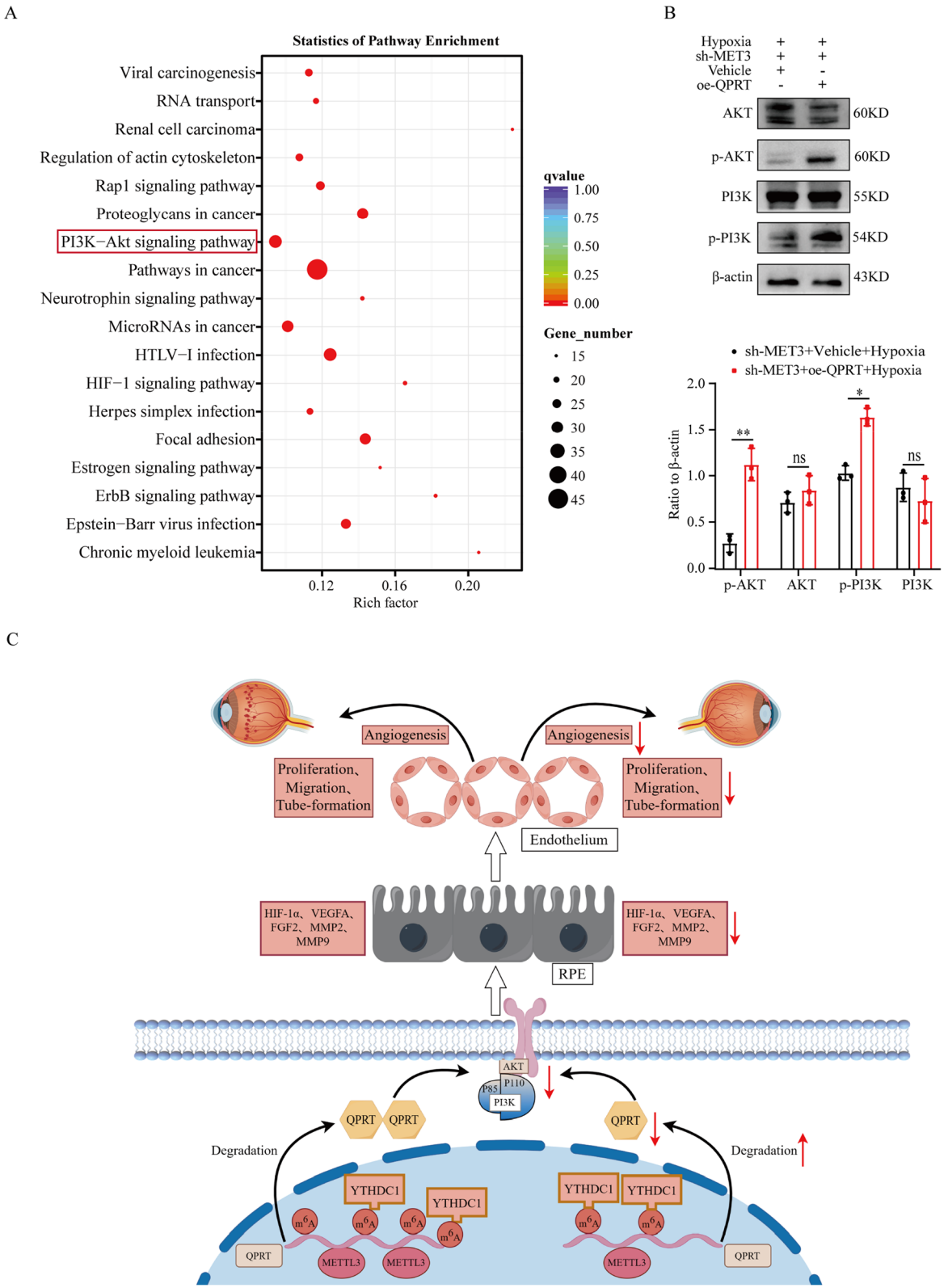

Fig. 6 Mechanistic network diagram of the role of METTL3 in angiogenesis. **A** Enrichment assessment of KEGG pathways for genes exhibiting differential expression. **B** Representative western blotting images of p-PI3K, PI3K, p-AKT, and AKT in METTL3-silenced cells subjected to vehicle or oe-QPRT after 24 h of hypoxia stimulation (n = 3; mean ± SD; ns > 0.05; *p < 0.05, **p < 0.01; unpaired Student's t-test). **C** Graphical summary of this study

Supplementary Information

The online version contains supplementary material available at https://doi.org/10.1186/s12974-024-03279-1.

Supplementary material 1.

Acknowledgements
We are immensely grateful for the floxed Mettl3 mice generously provided by Professor Xianjun Zhu.

Author contributions
QZ and XL designed this study and wrote this manuscript; HL performed bioanalysis; NL, JM and JH searched literature and revised the manuscript; ZZ, JL, WF, WL, and XL contributed reagents, materials and analysis tools; XL and HZ analyzed data; PY and SH helped to conceive the research and revise the manuscript. All authors reviewed the manuscript.

Funding
This work was supported by the National Natural Science Foundation Project of China (82070951, 82271078), Beijing Municipal Public Welfare Development and Reform Pilot Project for Medical Research Institutes (PWD&RPP-MRI, JYY2023-6) and Young Scholars of Beijing.

Availability of data and materials
No datasets were generated or analysed during the current study.

Declarations

Competing interests
The authors declare no competing interests.

Received: 13 September 2024 Accepted: 28 October 2024
Published online: 06 November 2024

References

1. McAnally D, Siddiquee K, Gomaa A, Szabo A, Vasile S, Maloney PR, et al. Repurposing antimalarial aminoquinolines and related compounds for treatment of retinal neovascularization. PLoS ONE. 2018;13(9):e0202436.
2. Li X, Wang G, Li N, Wang X, Fan W, Zhang Z, et al. Icariin alleviates oxygen-induced retinopathy by targeting microglia hexokinase 2. Immunology. 2024;173(1):141–51.
3. Patel NA, Acaba-Berrocal LA, Hoyek S, Fan KC, Martinez-Castellanos MA, Baumal CR, et al. Practice patterns and outcomes of intravitreal Anti-VEGF injection for retinopathy of prematurity: an international multicenter study. Ophthalmology. 2022;129(12):1380–8.
4. Tsai AS, Chou HD, Ling XC, Al-Khaled T, Valikodath N, Cole E, et al. Assessment and management of retinopathy of prematurity in the era of anti-vascular endothelial growth factor (VEGF). Prog Retin Eye Res. 2022;88:101018.
5. Tsai CY, Yeh PT, Tsao PN, Chung YE, Chang YS, Lai TT. Neurodevelopmental outcomes after bevacizumab treatment for retinopathy of prematurity: a meta-analysis. Ophthalmology. 2021;128(6):877–88.
6. Arrigo A, Aragona E, Bandello F. VEGF-targeting drugs for the treatment of retinal neovascularization in diabetic retinopathy. Ann Med. 2022;54(1):1089–111.
7. Grossniklaus HE, Kang SJ, Berglin L. Animal models of choroidal and retinal neovascularization. Prog Retin Eye Res. 2010;29(6):500–19.
8. Lin M, Hu Y, Chen Y, Zhou KK, Jin J, Zhu M, et al. Impacts of hypoxia-inducible factor-1 knockout in the retinal pigment epithelium on choroidal neovascularization. Invest Ophthalmol Vis Sci. 2012;53(10):6197–206.
9. Xu Z, Liao X, Li N, Zhou H, Li H, Zhang Q, et al. A single-cell transcriptome atlas of the human retinal pigment epithelium. Front Cell Dev Biol. 2021;9:802457.
10. Reichhart N, Strauss O. Ion channels and transporters of the retinal pigment epithelium. Exp Eye Res. 2014;126:27–37.
11. Han JW, Lyu J, Park YJ, Jang SY, Park TK. Wnt/β-Catenin signaling mediates regeneration of retinal pigment epithelium after laser photocoagulation in mouse eye. Invest Ophthalmol Vis Sci. 2015;56(13):8314–24.
12. Liu X, Meng J, Liao X, Liu Y, Zhou Q, Xu Z, et al. A de novo missense mutation in MPP2 confers an increased risk of Vogt-Koyanagi-Harada disease as shown by trio-based whole-exome sequencing. Cell Mol Immunol. 2023;20(11):1379–92.
13. Jarrett SG, Boulton ME. Consequences of oxidative stress in age-related macular degeneration. Mol Aspects Med. 2012;33(4):399–417.
14. Hanus J, Anderson C, Wang S. RPE necroptosis in response to oxidative stress and in AMD. Ageing Res Rev. 2015;24(Pt B):286–98.
15. Binder S, Stanzel BV, Krebs I, Glittenberg C. Transplantation of the RPE in AMD. Prog Retin Eye Res. 2007;26(5):516–54.
16. Chen W, He S, Xiang D. Hypoxia-induced retinal pigment epithelium cell-derived bFGF promotes the migration and angiogenesis of HUVECs through regulating TGF-β1/smad2/3 pathway. Gene. 2021;790:145695.
17. Hoffmann S, He S, Ehren M, Ryan SJ, Wiedemann P, Hinton DR. MMP-2 and MMP-9 secretion by rpe is stimulated by angiogenic molecules found in choroidal neovascular membranes. Retina. 2006;26(4):454–61.
18. Tang S, Meng J, Tan J, Liu X, Zhou H, Li N, et al. N6-methyladenosine demethylase FTO regulates inflammatory cytokine secretion and tight junctions in retinal pigment epithelium cells. Clin Immunol. 2022;241:109080.
19. Meng J, Liu X, Tang S, Liu Y, Zhao C, Zhou Q, et al. METTL3 inhibits inflammation of retinal pigment epithelium cells by regulating NR2F1 in an m(6)A-dependent manner. Front Immunol. 2022;13:905211.
20. Sendinc E, Shi Y. RNA m6A methylation across the transcriptome. Mol Cell. 2023;83(3):428–41.
21. Bai L, Xiang Y, Tang M, Liu S, Chen Q, Chen Q, et al. ALKBH5 controls the meiosis-coupled mRNA clearance in oocytes by removing the N (6)-methyladenosine methylation. Nat Commun. 2023;14(1):6532.
22. Zhang Z, Wang XJ. N(6)-Methyladenosine mRNA modification: from modification site selectivity to neurological functions. Acc Chem Res. 2023;56(21):2992–9.
23. Niu Y, Zhao X, Wu YS, Li MM, Wang XJ, Yang YG. N6-methyl-adenosine (m6A) in RNA: an old modification with a novel epigenetic function. Genomics Proteomics Bioinformatics. 2013;11(1):8–17.
24. Shi H, Wei J, He C. Where, when, and how: context-dependent functions of rna methylation writers, readers, and erasers. Mol Cell. 2019;74(4):640–50.
25. Wang L, Hui H, Agrawal K, Kang Y, Li N, Tang R, et al. m(6) A RNA methyltransferases METTL3/14 regulate immune responses to anti-PD-1 therapy. EMBO J. 2020;39(20):e104514.
26. Chen Y, Lu Z, Qi C, Yu C, Li Y, Huan W, et al. N(6)-methyladenosine-modified TRAF1 promotes sunitinib resistance by regulating apoptosis and angiogenesis in a METTL14-dependent manner in renal cell carcinoma. Mol Cancer. 2022;21(1):111.
27. Mendel M, Chen KM, Homolka D, Gos P, Pandey RR, McCarthy AA, et al. Methylation of structured RNA by the m(6)A writer METTL16 is essential for mouse embryonic development. Mol Cell. 2018;71(6):986-1000.e11.
28. Geula S, Moshitch-Moshkovitz S, Dominissini D, Mansour AA, Kol N, Salmon-Divon M, et al. Stem cells. m6A mRNA methylation facilitates resolution of naïve pluripotency toward differentiation. Science. 2015;347(6225):1002–6.
29. Wang W, Ye W, Chen S, Tang Y, Chen D, Lu Y, et al. METTL3-mediated m(6) A RNA modification promotes corneal neovascularization by upregulating the canonical Wnt pathway during HSV-1 infection. Cell Signal. 2023;109:110784.
30. Simão S, Santos DF, Silva GA. Aliskiren decreases oxidative stress and angiogenic markers in retinal pigment epithelium cells. Angiogenesis. 2017;20(1):175–81.
31. Chen HM, Li H, Lin MX, Fan WJ, Zhang Y, Lin YT, et al. Research progress for rna modifications in physiological and pathological angiogenesis. Front Genet. 2022;13:952667.
32. Yue SW, Liu HL, Su HF, Luo C, Liang HF, Zhang BX, et al. m6A-regulated tumor glycolysis: new advances in epigenetics and metabolism. Mol Cancer. 2023;22(1):137.
33. Yankova E, Blackaby W, Albertella M, Rak J, De Braekeleer E, Tsagkogeorga G, et al. Small-molecule inhibition of METTL3 as a strategy against myeloid leukaemia. Nature. 2021;593(7860):597–601.
34. Zhang ZW, Teng X, Zhao F, Ma C, Zhang J, Xiao LF, et al. METTL3 regulates m(6)A methylation of PTCH1 and GLI2 in Sonic hedgehog signaling

to promote tumor progression in SHH-medulloblastoma. Cell Rep. 2022;41(4):111530.
35. Connor KM, Krah NM, Dennison RJ, Aderman CM, Chen J, Guerin KI, et al. Quantification of oxygen-induced retinopathy in the mouse: a model of vessel loss, vessel regrowth and pathological angiogenesis. Nat Protoc. 2009;4(11):1565–73.
36. Smith LE, Wesolowski E, McLellan A, Kostyk SK, D'Amato R, Sullivan R, et al. Oxygen-induced retinopathy in the mouse. Invest Ophthalmol Vis Sci. 1994;35(1):101–11.
37. Sahm F, Oezen I, Opitz CA, Radlwimmer B, von Deimling A, Ahrendt T, et al. The endogenous tryptophan metabolite and NAD+ precursor quinolinic acid confers resistance of gliomas to oxidative stress. Cancer Res. 2013;73(11):3225–34.
38. Ishidoh K, Kamemura N, Imagawa T, Oda M, Sakurai J, Katunuma N. Quinolinate phosphoribosyl transferase, a key enzyme in de novo NAD(+) synthesis, suppresses spontaneous cell death by inhibiting overproduction of active-caspase-3. Biochem Biophys Acta. 2010;1803(5):527–33.
39. Liu CL, Cheng SP, Chen MJ, Lin CH, Chen SN, Kuo YH, et al. Quinolinate phosphoribosyltransferase promotes invasiveness of breast cancer through myosin light chain phosphorylation. Front Endocrinol. 2020;11:621944.
40. Stoilov P, Rafalska I, Stamm S. YTH: a new domain in nuclear proteins. Trends Biochem Sci. 2002;27(10):495–7.
41. Liao J, Wei Y, Liang J, Wen J, Chen X, Zhang B, et al. Insight into the structure, physiological function, and role in cancer of m6A readers-YTH domain-containing proteins. Cell Death Discov. 2022;8(1):137.
42. Zhou L, Mu L, Jiang W, Yang Q. QPRT acts as an independent prognostic factor in invasive breast cancer. J Oncol. 2022;2022:6548644.
43. Niu YC, Tong J, Shi XF, Zhang T. MicroRNA-654-3p enhances cisplatin sensitivity by targeting QPRT and inhibiting the PI3K/AKT signaling pathway in ovarian cancer cells. Exp Ther Med. 2020;20(2):1467–79.
44. Xu Y, Cui K, Li J, Tang X, Lin J, Lu X, et al. Melatonin attenuates choroidal neovascularization by regulating macrophage/microglia polarization via inhibition of RhoA/ROCK signaling pathway. J Pineal Res. 2020;69(1):e12660.
45. Wang X, Fan W, Li N, Ma Y, Yao M, Wang G, et al. YY1 lactylation in microglia promotes angiogenesis through transcription activation-mediated upregulation of FGF2. Genome Biol. 2023;24(1):87.
46. Rattner A, Williams J, Nathans J. Roles of HIFs and VEGF in angiogenesis in the retina and brain. J Clin Investig. 2019;129(9):3807–20.
47. Zhao X, Gao M, Liang J, Chen Y, Wang Y, Wang Y, et al. SLC7A11 reduces laser-induced choroidal neovascularization by inhibiting RPE ferroptosis and VEGF production. Front Cel Dev Biol. 2021;9:639851.
48. Liu X, Zhou Q, Meng J, Zuo H, Li R, Zhang R, et al. Autophagy-mediated activation of the AIM2 inflammasome enhances M1 polarization of microglia and exacerbates retinal neovascularization. MedComm. 2024;5(8):e668.
49. Chen X, Gong W, Shao X, Shi T, Zhang L, Dong J, et al. METTL3-mediated m(6)A modification of ATG7 regulates autophagy-GATA4 axis to promote cellular senescence and osteoarthritis progression. Ann Rheum Dis. 2022;81(1):87–99.
50. Yu J, Chai P, Xie M, Ge S, Ruan J, Fan X, et al. Histone lactylation drives oncogenesis by facilitating m(6)A reader protein YTHDF2 expression in ocular melanoma. Genome Biol. 2021;22(1):85.
51. Liu J, Huang T, Yao J, Zhao T, Zhang Y, Zhang R. Epitranscriptomic subtyping, visualization, and denoising by global motif visualization. Nat Commun. 2023;14(1):5944.
52. Luo Z, Ma Q, Sun S, Li N, Wang H, Ying Z, et al. Exon-intron boundary inhibits m(6)A deposition, enabling m(6)A distribution hallmark, longer mRNA half-life and flexible protein coding. Nat Commun. 2023;14(1):4172.
53. Wang G, Dai Y, Li K, Cheng M, Xiong G, Wang X, et al. Deficiency of Mettl3 in bladder cancer stem cells inhibits bladder cancer progression and angiogenesis. Front Cell Dev Biol. 2021;9:627706.
54. Han J, Wang JZ, Yang X, Yu H, Zhou R, Lu HC, et al. METTL3 promote tumor proliferation of bladder cancer by accelerating pri-miR221/222 maturation in m6A-dependent manner. Mol Cancer. 2019;18(1):110.
55. Shan K, Zhou RM, Xiang J, Sun YN, Liu C, Lv MW, et al. FTO regulates ocular angiogenesis via m(6)A-YTHDF2-dependent mechanism. Exp Eye Res. 2020;197:108107.
56. Tian C, Huang Y, Li Q, Feng Z, Xu Q. Mettl3 regulates osteogenic differentiation and alternative splicing of vegfa in bone marrow mesenchymal stem cells. Int J Mol Sci. 2019;20(3):551.
57. Garcia-Ramírez M, Hernández C, Ruiz-Meana M, Villarroel M, Corraliza L, García-Dorado D, et al. Erythropoietin protects retinal pigment epithelial cells against the increase of permeability induced by diabetic conditions: essential role of JAK2/ PI3K signaling. Cell Signal. 2011;23(10):1596–602.
58. Li Y, Liu X, Zhou T, Kelley MR, Edwards P, Gao H, et al. Inhibition of APE1/ Ref-1 redox activity rescues human retinal pigment epithelial cells from oxidative stress and reduces choroidal neovascularization. Redox Biol. 2014;2:485–94.
59. Hayreh SS. Neovascular glaucoma. Prog Retin Eye Res. 2007;26(5):470–85.

Publisher's Note

Springer Nature remains neutral with regard to jurisdictional claims in published maps and institutional affiliations.